SIBS-Based Biocompatible Nanocomposites

Subjects: Materials Science, Biomaterials

Contributor: Maria A. Rezvova , Arseniy E. Yuzhalin , Tatiana V. Glushkova , Miraslau I. Makarevich , Pavel A. Nikishau , Sergei V. Kostjuk , Kirill Yu. Klyshnikov , Vera G. Matveeva , Mariam Yu. Khanova , Evgeny A. Ovcharenko

Carbon nanotubes (CNTs) were incorporated into poly(styrene-block-isobutyleneblock-styrene) (SIBS) to investigate the physical characteristics of the resulting nanocomposite and its cytotoxicity to endothelial cells. CNTs were dispersed in chloroform using sonication following the addition of a SIBS solution at different ratios. We observed an uneven distribution of CNTs in the polymer matrix with sporadic bundles of interwoven nanotubes. Increasing the CNT content from 0 wt% to 8 wt% led to an increase in the tensile strength of SIBS films from 4.69 to 16.48 MPa. The engineering normal strain significantly decreased in 1 wt% SIBS–CNT films in comparison with the unmodified samples, whereas a further increase in the CNT content did not significantly affect this parameter. The incorporation of CNT into the SIBS matrix resulted in increased hydrophilicity, whereas no cytotoxicity towards endothelial cells was noted.

nanocomposites carbon nanotubes biocompatible materials electrical conductivity triblock copolymers

1. Introduction

Carbon-based nanomaterials are currently actively tested for their potential usefulness in the modification of implantable medical devices [1][2], owing to their extraordinary high tensile strength which is attributed to the special organization of carbon atoms in a two-dimensional hexagonal grid [3]. Such cellular structure is characteristic of graphene and other allotropic modifications of carbon with sp^2 hybridization such as fullerene and carbon nanotubes (CNTs).

The incorporation of carbon-based nanomaterials into polymer structure greatly enhances its mechanical properties, specifically tensile strength [4][5], which is of the upmost importance for implantable medical devices used in CVD, including vascular substitutes, chords, patches, and heart valves. On the other hand, the presence of carbon-based nanomaterials may lead to the reduced elasticity and increased rigidity of the final device, thus adversely affecting its function [6][7]. However, CNTs representing the coiled layers of graphene can be a promising material for the manufacture of implantable devices, owing to their flexibility and high tensile strength of about 50–150 GPa [8]. In addition to enhanced tensile strength, carbon-based nanomaterials may endow polymers with antimicrobial activity, electrical conductivity, or even improved hemocompatibility [9][10]. All of the above could be beneficial for implantable medical devices prone to thrombogenicity and infections.

2. Synthesis of CNT-Modified SIBS Films and Analysis of Their Structure

Triblock copolymers of isobutylene with styrene (M_n = 50,000 g/mol, M_w/M_n < 1.3, central polyisobutylene block M_n = 36,000 g/mol, M_w/M_n < 1.2) were synthesized by the sequential controlled cationic polymerization of isobutylene and styrene, employing the dicumyl chloride/$TiCl_4$/2,6-dimethylpyridine initiating system at −80 °C. The gel permeation chromatography (GPC) curve of polyisobutylene completely shifts to the high molecular weight region after the addition of the second monomer (styrene) into the polymerization mixture, thus confirming the successful formation of the desired triblock copolymer (Figure 1A). The ^{1}H NMR spectra of SIBS (Figure 1B) exhibited well resolved signals corresponding to the phenyl protons (6.2–7.2 ppm, *b*) of the polystyrene block and methyl protons (1.0–1.2 ppm, *c*) of the polyisobutylene block. In addition to these signals, the spectra showed lower intensity resonances corresponding to the methyl protons of the first isobutylene unit attached to the initiator at 0.78 ppm (*d*) and terminal chloromethine protons at 4.2–4.5 ppm (*a*). The weight fraction of polystyrene in SIBS was calculated from the integral intensities of the corresponding signals and was 32%, which is very close to the weight fraction of styrene in the initial comonomers mixture (33%). The resultant copolymer was further used for CNT incorporation.

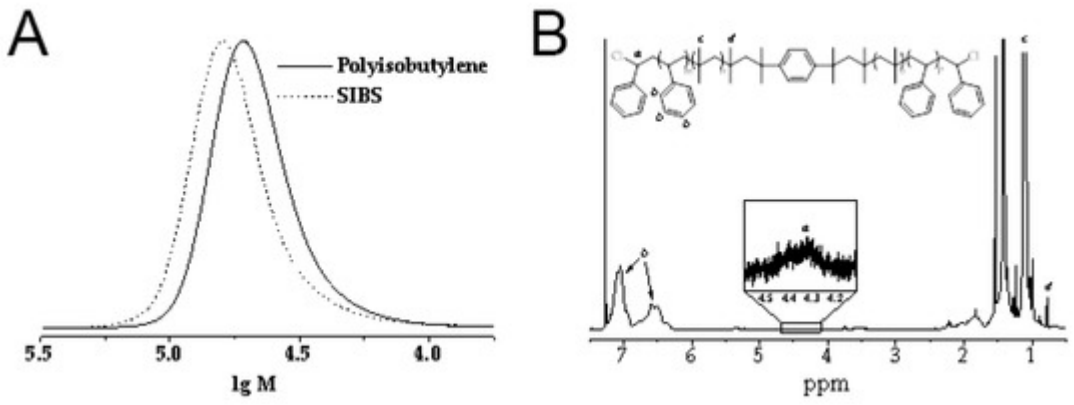

Figure 1. (**A**). Gel permeation chromatography (GPC) curves of the polyisobutylene middle block and the SIBS block-copolymer. (**B**). ^{1}H NMR spectra of resultant copolymers.

Ultrasound-dispersed CNTs in chloroform and polymer solution were stable under static conditions at room temperature for 2 weeks. The SIBS solutions of different CNT concentrations (1%, 2%, 4%, 6%, and 8%) were cast to obtain nanocomposite films, which exhibited a homogenous structure and had a thickness of 100 ± 5 µm.

An ATR-FTIR spectrum of the resultant films (Figure 2) matched with previously reported SIBS spectra [11]. An absorbance peak at 2952 cm^{-1} corresponded to the asymmetric stretching vibrations of aliphatic –CH_3 groups of isobutylene, while peaks at 2915–2847 cm^{-1} were determined by symmetric stretching vibrations of aliphatic –CH_3 groups. The 1463 cm^{-1} peak was characteristic of the bending vibrations of aliphatic –CH_2 and –CH_3 groups. Absorbance peaks at 1373 and 1227 cm^{-1} correspond to the –CH_3 groups of aliphatic chains and stretching vibrations of C–C bonds in the carbon backbone, respectively. The 1009 cm^{-1} peak reflected the stretching vibrations of C–C bonds in the carbon backbone. An increase in the CNT content led to a gradual reduction in the

intensity of these absorption peaks due to the scattering of the reflected energy. The wide peak at 1600 cm^{-1} could be attributed to C–C vibrations in CNTs [12].

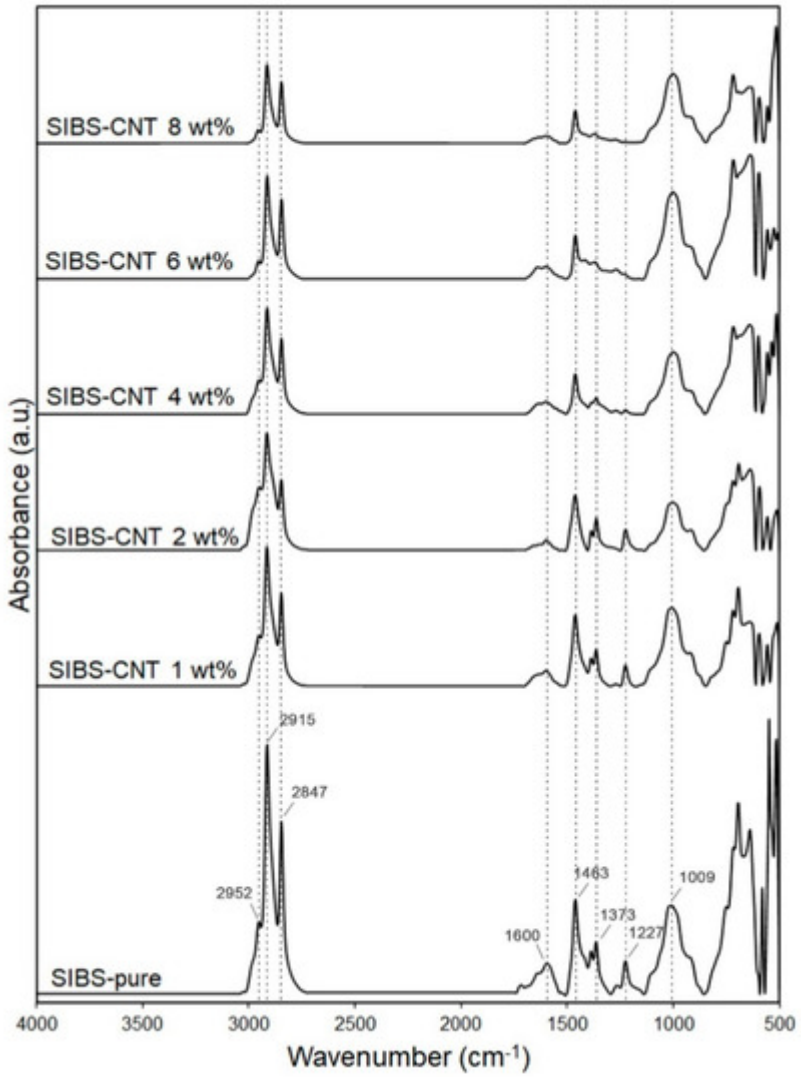

Figure 2. FTIR spectra of the intact and carbon nanotube (CNT)-modified SIBS.

When analyzing the structure of SIBS–CNT films by optical microscopy, we observed a relatively uniform distribution of particles within the polymer matrix; however, sporadic CNT inclusions of a significant size exceeding the nanoscale level were observed in all CNT-modified SIBS samples (Figure 3). In certain areas, CNTs formed fiber networks characterized as bundles of interwoven nanotubes. An increase in the CNT content led to a gradual reduction in the films' optical transparency and an increase in the number of CNT agglomerates (Figure 3A–F). The scanning electron microscopy (SEM) analysis of the nanocomposites' surface showed a minimal difference between the intact CNT-modified SIBS films (Figure 3G–L); specifically, the unmodified SIBS had a regular surface pattern, whereas the SIBS–CNT films exhibited irregular depressions and elevations.

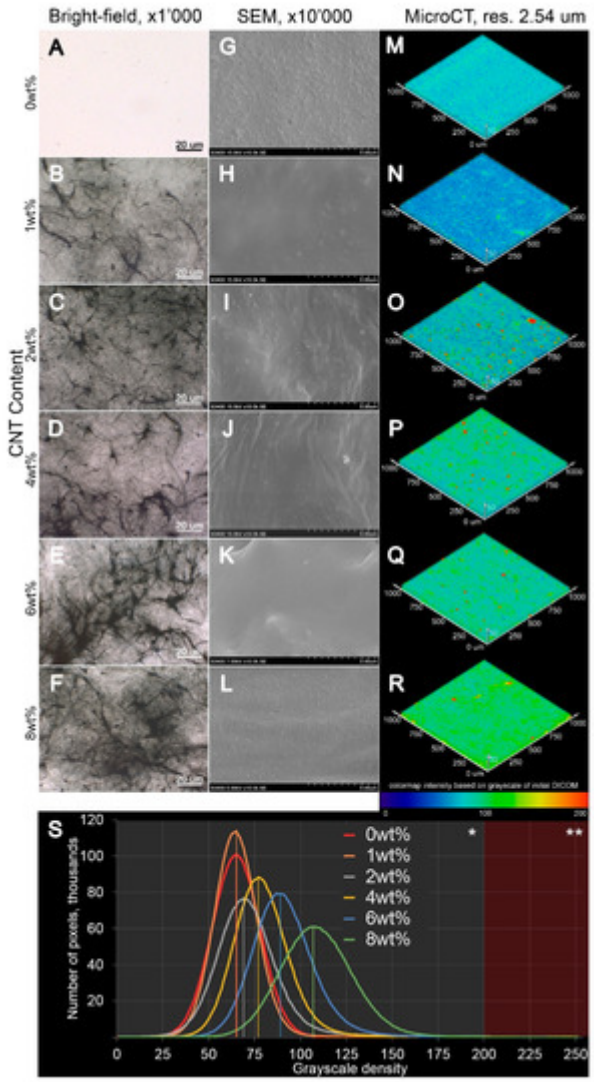

Figure 3. (**A**–**L**). Representative images of the intact and CNT-modified SIBS films acquired using optical (**A**–**F**), ×1000 magnification, and scanning electron microscopy (**G**–**L**), ×10,000 magnification. (**M**–**R**). The 3D reconstruction images of CNT distribution in SIBS films of 1000 µm height × 1000 µm length × 50 depth. For clarity, the visualization of 3D reconstructions was performed in the range of 0–200 units of X-ray density as the most informative, i.e., containing >99% of all pixels. The range of 201–255 units was excluded (contains <1% of all pixels). (**S**). The effect of CNT concentration on the X-ray density of SIBS films.

The analysis of films by micro-CT showed that the weighted average basic density of the unmodified SIBS was 65 units (range: 42–86 grayscale units based on 95% pixels). The addition of CNTs led to a gradual increase in the weighted average density, with the most prominent increment of density at CNT concentrations of >4 wt% (Figure 3S). An increase in CNT content was associated with a higher standard deviation of density, indicating an uneven distribution of CNTs. Qualitatively, the 3D reconstruction of CNT distribution revealed two distinct forms of particles within SIBS–CNT films: (i) CNTs uniformly dispersed in SIBS and (ii) CNT agglomerates of >10 µm^3 (Figure 3M–R). Notably, both (i) and (ii) were found in all SIBS–CNT films regardless of their CNT concentration.

3. Tensile Testing of CNT-Modified SIBS Films

All the CNT-modified SIBS films demonstrated a significantly higher ultimate tensile strength as compared to unmodified SIBS samples ($p < 0.01$) (Figure 4A). Increasing the CNT content from 0 wt% to 4 wt% led to a linear increase in the Young's modulus of SIBS films (Figure 4B). Upon reaching the CNT concentration of 4 wt%, the Young's modulus soared to 52.7 MPa, which is 12 times higher than that of unmodified SIBS samples. In samples with a CNT concentration of 6 wt% and 8%, an even more dramatic rise in the Young's modulus was documented (Figure 4B). The uniform elongation demonstrated a sharp drop in 1 wt% SIBS–CNT films in comparison with unmodified samples ($p < 0.0001$) (Figure 4C), while a further increase in the CNT content did not significantly affect this parameter.

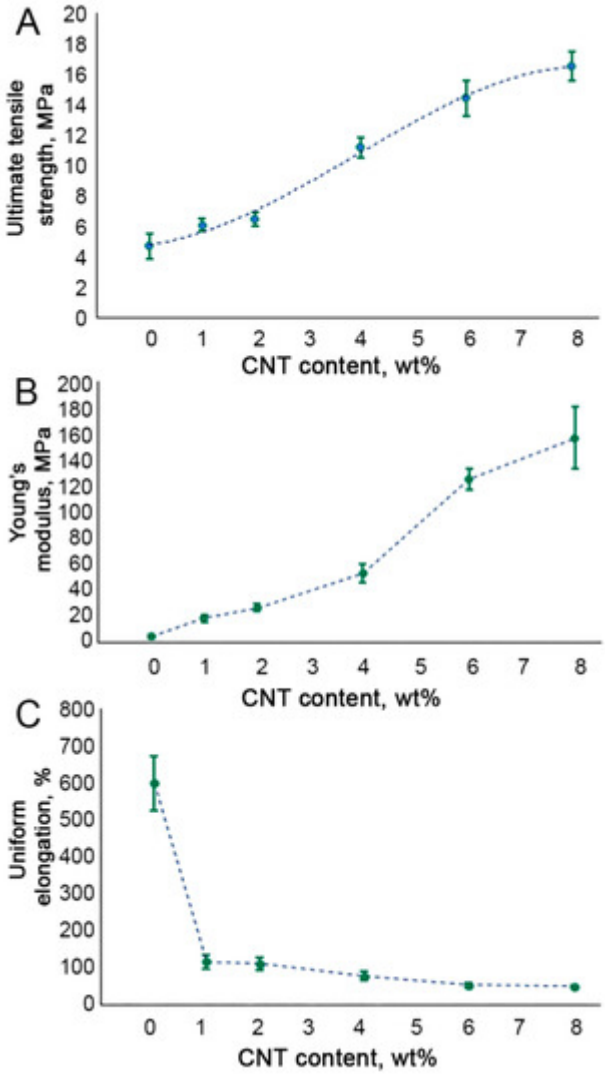

Figure 4. Tensile testing of SIBS–CNT films of different nanofiller concentrations: (**A**). the ultimate tensile strength; (**B**). Young's modulus; (**C**). uniform elongation.

4. Hydrophobicity Assessment of CNT-Modified SIBS Films

The incorporation of CNTs into the SIBS matrix resulted in a gradual reduction of the wetting angle, suggesting increased hydrophilicity (Figure 5). Although SIBS films with a CNT concentration of 1 wt% and 2 wt% demonstrated a similar wetting angle to that of control SIBS samples (all above 90°), a further CNT increase to 4 wt%, 6 wt% and 8 wt% led to a progressive reduction of the wetting angle to 84.4° ± 2.3°, 63.9° ± 3.2° and 66.7° ± 5.2°, respectively. Since materials with a contact angle below 90° can be considered as hydrophilic [13], 4 wt%, 6 wt% and 8 wt% SIBS–CNT films were characterized as hydrophilic in comparison with hydrophobic control SIBS samples.

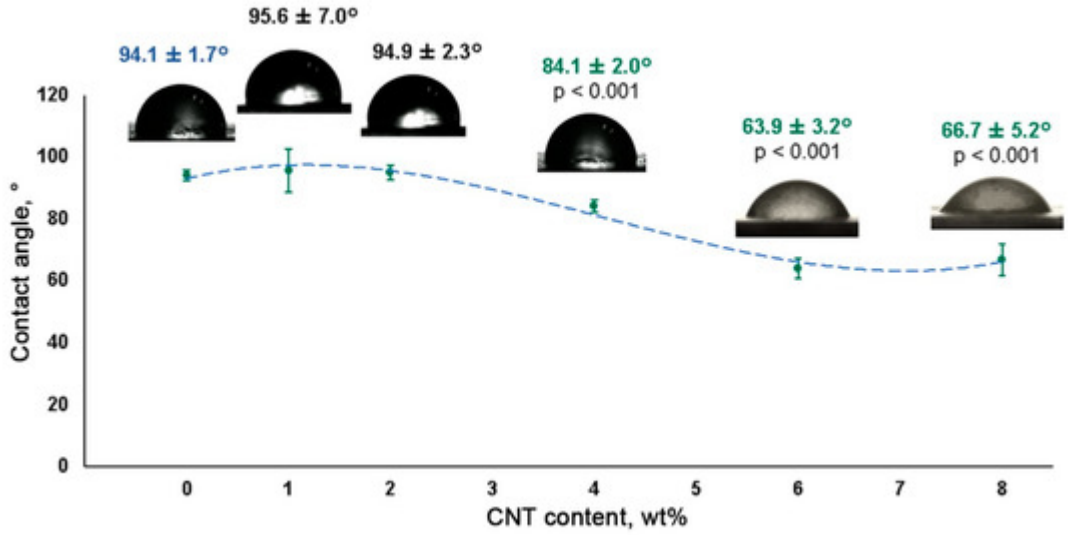

Figure 5. Water contact angles of SIBS–CNT films of different nanofiller concentrations.

5. Electrical Conductivity Measurement of CNT-Modified SIBS Films

The high electrical conductivity of a material is a requirement for the development of heart muscle patches [14]. An increase in CNT content resulted in the elevated electrical conductivity of SIBS–CNT films from 0.07 S/cm at 1 wt% CNT to 8.55 S/cm at 8 wt% CNT (Figure 6). Considering the insulating properties of the unmodified SIBS (approximately 10^{-14} S/cm), it can be concluded that CNT incorporation led to a substantial (about 10^4 S/cm) increase in the electrical conductivity of the nanocomposite.

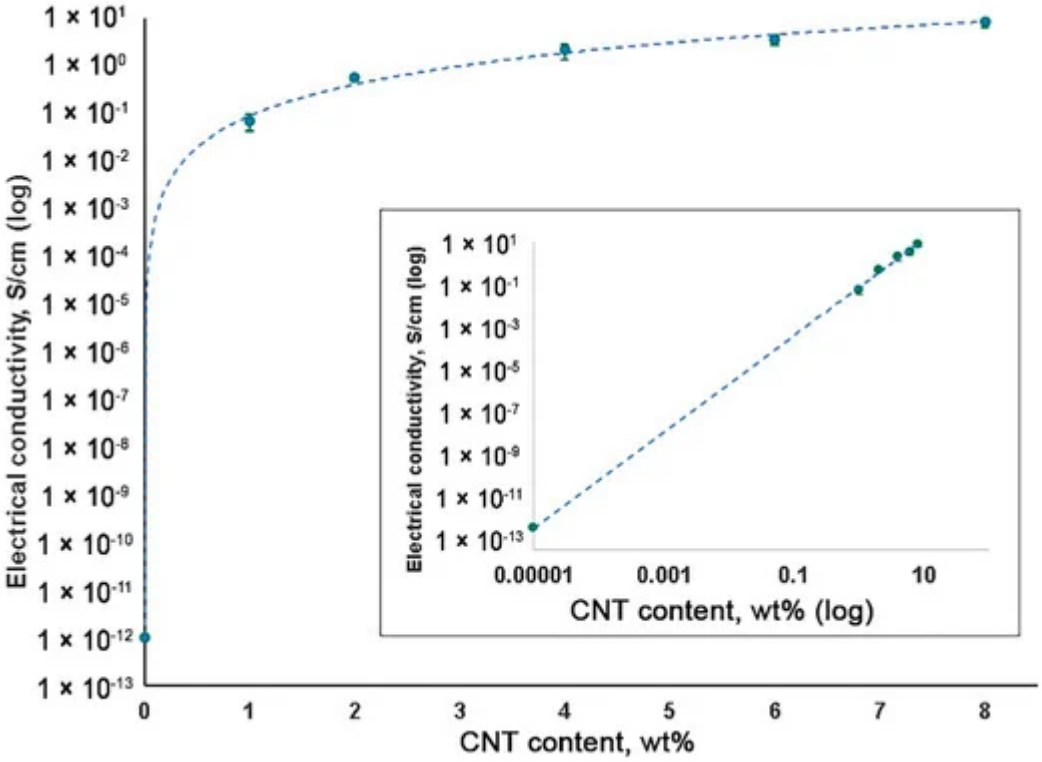

Figure 6. Electrical conductivity of SIBS–CNT films of different nanofiller concentrations.

6. Cytotoxicity of CNT-Modified SIBS Films

To evaluate the potential cytotoxicity of CNT-modified SIBS films, we immobilized them on cell culture plates to investigate the growth of HUVECs on their surface. Three days post seeding, the absolute number (per 1 mm^2) of HUVECs cultured on SIBS films regardless of CNT incorporation was significantly reduced in comparison with those grown in lab plastic ($p < 0.05$) (Figure 7). This suggests a slower growth of HUVECs on SIBS films. Notably, the incorporation of CNTs into SIBS did not affect HUVEC growth (Figure 7A,B). The relative number of viable cells was nearly identical in all study groups except for the positive control where the cells were treated with pure CNTs ($p < 0.05$) (Figure 7C). Thus, these data suggest that CNT-modified SIBS films exhibit cytotoxicity comparable to that of culture plastic and can therefore be considered biocompatible.

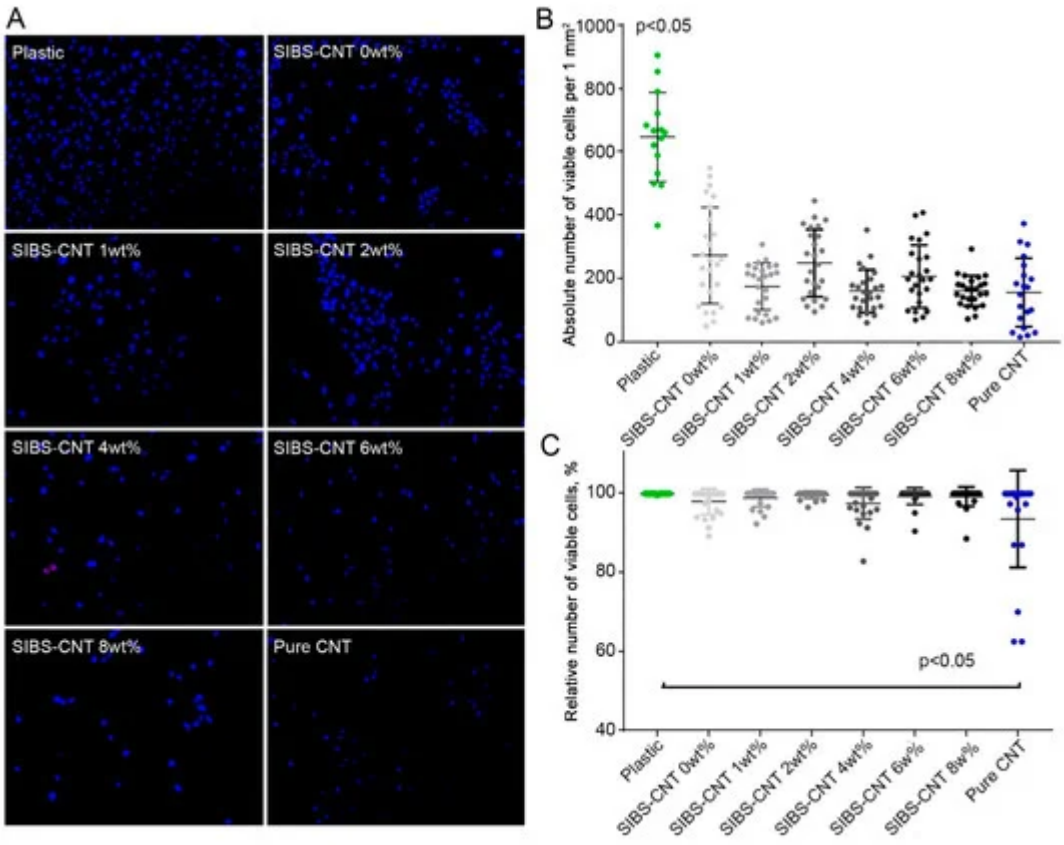

Figure 7. (**A**). Representative images of human umbilical vein endothelial cells (HUVEC) cultured on SIBS–CNT films for 3 days. Cells were stained with Hoechst (blue) and ethidium bromide (red). (**B**). The quantification of the cell number per mm^2 of SIBS–CNT surface in the indicated groups. (**C**). Percentage of the viable cells in the indicated groups.

7. In Vitro Oxidative Stability of CNT-Modified SIBS Films

To evaluate the stability of CNT-modified SIBS films, we performed an in vitro oxidation assay by submerging the samples in a solution of 0.1 M $CoCl_2$ in 20% H_2O_2 for 14 days. We did not observe any evidence of corrosion or cracking over the course of the experiment, suggesting that both intact and CNT-modified SIBS are resistant to oxidative degradation (Figure 8A). However, the oxidative stress led in the formation of a new IR peak at 1724 cm^{-1}, which is characteristic of stretching vibrations of C=O or –COOH bonds (Figure 8B).

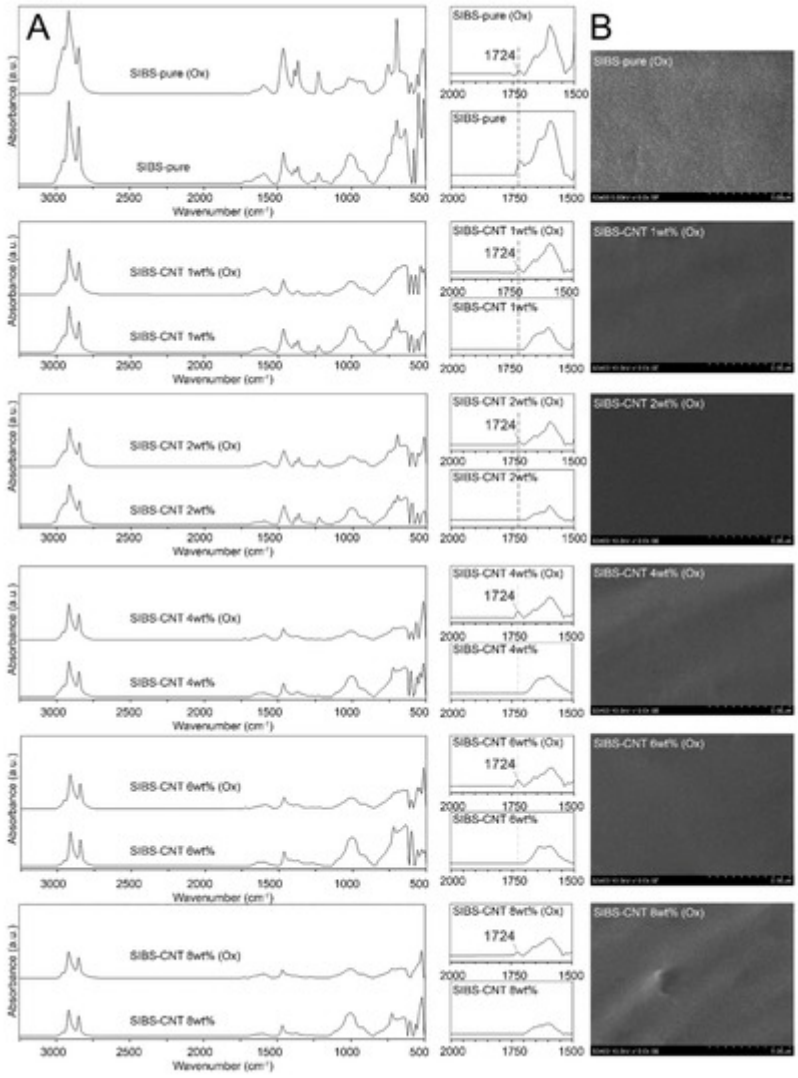

Figure 8. (**A**). SEM images of the surface of intact and CNT-modified SIBS films after 14 days of oxidation stress. (**B**). FTIR spectra of intact and CNT-modified SIBS films before and after 14 days of oxidation stress.

8. Conclusions

The incorporation of 8 wt% CNT into the SIBS matrix resulted in a significantly improved tensile strength and electrical conductivity, however, the high rigidity of this nanocomposite may limit its functionality. The most optimal results were documented for SIBS films with a CNT content of 4–6 wt%, which exhibited both high tensile strength and conductivity.

References

1. Farzana Hussain; Mehdi Hojjati; Masami Okamoto; Russell E. Gorga; Review article: Polymer-matrix Nanocomposites, Processing, Manufacturing, and Application: An Overview. *Journal of Composite Materials* **2006**, *40*, 1511-1575, 10.1177/0021998306067321.

2. Debabrata Maiti; Xiangmin Tong; Xiaozhou Mou; Kai Yang; Carbon-Based Nanomaterials for Biomedical Applications: A Recent Study. *Frontiers in Pharmacology* **2019**, *9*, 1401, 10.3389/fphar.2018.01401.
3. Ali Eatemadi; Hadis Daraee; Hamzeh Karimkhanloo; Mohammad Kouhi; Nosratollah Zarghami; Abolfazl Akbarzadeh; Mozhgan Abasi; Younes Hanifehpour; Sang Woo Joo; Carbon nanotubes: properties, synthesis, purification, and medical applications. *Nanoscale Research Letters* **2014**, *9*, 393-393, 10.1186/1556-276x-9-393.
4. Soad Z. Al Sheheri; Zahra M. Al-Amshany; Qana A. Al Sulami; Nada Y. Tashkandi; Mahmoud A. Hussein; Reda M. El-Shishtawy; The preparation of carbon nanofillers and their role on the performance of variable polymer nanocomposites. *Designed Monomers and Polymers* **2019**, *22*, 8-53, 10.1080/15685551.2019.1565664.
5. Pb Kalakonda; S Banne; Enhanced mechanical properties of multiwalled carbon nanotubes/thermoplastic polyurethane nanocomposites. *Nanomaterials and Nanotechnology* **2019**, *9*, 184798041984085, 10.1177/1847980419840858.
6. Alfred J. Crosby; Jong-Young Lee; Polymer Nanocomposites: The “Nano” Effect on Mechanical Properties. *Polymer Reviews* **2007**, *47*, 217-229, 10.1080/15583720701271278.
7. S.C. Tjong; Structural and mechanical properties of polymer nanocomposites. *Materials Science and Engineering: R: Reports* **2006**, *53*, 73-197, 10.1016/j.mser.2006.06.001.
8. Mrinal Bhattacharya; Polymer Nanocomposites—A Comparison between Carbon Nanotubes, Graphene, and Clay as Nanofillers. *Materials* **2016**, *9*, 262, 10.3390/ma9040262.
9. H.A. Khan; M.K. Sakharkar; A. Nayak; U. Kishore; A. Khan; Nanoparticles for biomedical applications: An overview. *Nanobiomaterials* **2018**, *14*, 357-384, 10.1016/b978-0-08-100716-7.00014-3.
10. Ahmed Al-Jumaili; Surjith Alancherry; Kateryna Bazaka; Mohan V. Jacob; Review on the Antimicrobial Properties of Carbon Nanostructures. *Materials* **2017**, *10*, 1066, 10.3390/ma10091066.
11. Shuaishuai Yuan; Jie Zhao; Shifang Luan; Shunjie Yan; Wanling Zheng; Jinghua Yin; Nuclease-Functionalized Poly(Styrene-b-isobutylene-b-styrene) Surface with Anti-Infection and Tissue Integration Bifunctions. *ACS Applied Materials & Interfaces* **2014**, *6*, 18078-18086, 10.1021/am504955g.
12. Mohamed Abdel Salam; Abdullah Y. Obaid; Reda M. El-Shishtawy; Saleh A. Mohamed; Synthesis of nanocomposites of polypyrrole/carbon nanotubes/silver nano particles and their application in water disinfection. *RSC Advances* **2017**, *7*, 16878-16884, 10.1039/c7ra01033h.
13. Matej Kanduč; Alexander Schlaich; Emanuel Schneck; Roland R. Netz; Water-Mediated Interactions between Hydrophilic and Hydrophobic Surfaces. *Langmuir* **2016**, *32*, 8767-8782, 10.1

021/acs.langmuir.6b01727.

14. Matteo Solazzo; Fergal J. O'brien; Valeria Nicolosi; Michael G. Monaghan; The rationale and emergence of electroconductive biomaterial scaffolds in cardiac tissue engineering. *APL Bioengineering* **2019**, *3*, 041501, 10.1063/1.5116579.

Retrieved from https://encyclopedia.pub/entry/history/show/6457